가압축성 기법을 이용한 비정렬 격자상에서의 비압축성 점성해석
Incompressible Viscous Analysis on Unstructured Meshes using Artificial Compressibility Method

문 영 준[1]
Young J. Moon

Viscous analysis on incompressible flows is performed using unstructured triangular meshes. A two-dimensional and axisymmetric incompressible Navier-Stokes equations are solved in time-marching form by artificial compressibility method. The governing equations are discretized by a cell-centered based finite-volume method, and a centered scheme is used for inviscid and viscous fluxes with fourth order artificial dissipation. An explicit multi-stage Runge-Kutta method is used for the time integration with local time stepping and implicit residual smoothing. Convergence properties are examined and solution accuracies are also validated with benchmark solution and experiment.

1. Introduction

Recently attentions have been paid on unstructured algorithms in applications of calculating flows in complex geometries with automatic triangular mesh generation. On the other hand, there have been some issuses also, concerning on accuracies and convergences of the unstructured method. Some research efforts have been made for the validations of the unstructured schemes especially in high Reynolds number compressible flows. The present study is primarily focused on incompressible flows from low Reynolds number to moderate Reynolds numbers.

2. Mathematical Formulations

2.1 Governing Equations and Artificial Compressibility Method

Among the various methods in handling the incompressible Navier-Stokes equations, the artificial compressibility method is considered. This method was originally suggested by Chorin[1] and also extended by Kwak and Chang[2].

The axisymmetric incompressible Navier-Stokes equations are formulated in a time-marching hyperbolic form by artificial compressibility method as follows;

$$\frac{\partial Q}{\partial t}+\frac{\partial E}{\partial x}+\frac{\partial F}{\partial y}=\frac{\partial E_v}{\partial x}+\frac{\partial F_v}{\partial y}-H+H_v \tag{1}$$

where

$$Q=\begin{bmatrix} p \\ u \\ v \\ w \end{bmatrix},\quad E=\begin{bmatrix} \beta u \\ u^2+p \\ uv \\ uw \end{bmatrix},\quad F=\begin{bmatrix} \beta v \\ uv \\ v^2+p \\ vw \end{bmatrix},\quad E_v=\frac{1}{\mathrm{Re}}\begin{bmatrix} 0 \\ \partial u/\partial x \\ \partial v/\partial x \\ \partial w/\partial x \end{bmatrix},\quad F_v=\frac{1}{\mathrm{Re}}\begin{bmatrix} 0 \\ \partial u/\partial y \\ \partial v/\partial y \\ \partial w/\partial y \end{bmatrix}$$

$$H=\frac{1}{y}\begin{bmatrix} \beta v \\ uv \\ v^2-w^2 \\ 2vw \end{bmatrix},\qquad H_v=\frac{1}{\mathrm{Re}y}\begin{bmatrix} 0 \\ \partial u/\partial y \\ \partial v/\partial y-v/y \\ \partial w/\partial y-w/y \end{bmatrix} \tag{2}$$

and $\sqrt{\beta}$ is an artificial speed of sound such that $p=\beta\rho$. Eq. (1) returns to a two dimensional form by excluding the source vectors H and H_v and the last row in the equation.

[1]고려대학교 기계공학과(136-701, 성북구 안암동 5-1, Tel:02-920-1528)

2.2 Unstructured Finite Volume Method

A cell-centered based finite-volume form of discretization is applied by a volume integral to Eq. (1) on unstructured triangular meshes. Inviscid numerical fluxes at a cell face are defined by averaging of two nested cell values. Viscous fluxes are determined by two steps. First, gradients at a cell center are evaluated by a contour integral of the pre-calculated cell face values. Then the gradients at a cell face are averaged between two nested cells. Here an area-weighted rule is used in averagings. The numerical stencil of the present scheme is shown in Fig. 1. Also the fourth order artificial dissipation in a form suggested in Ref. [3] was used to ensure the stability of the centered scheme. The resulting equations are written in a discrete form as

$$\frac{\Delta Q_i}{\Delta t} V_i = -\sum_{j=k(i)} \left[(E-E_v)\Delta y - (F-F_v)\Delta x \right]_j - (H-H_v)_i V_i \qquad (3)$$

where i and j indicate the cell and its faces and $k(i)$ is the mapping relation between them. Also V_i denotes an area of the ith cell.

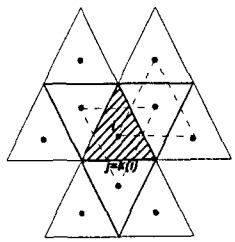

Fig. 1 10 points numerical stencil of the present scheme

2.3 *4* Stage Runge-Kutta Method

An explicit k-stage Runge-Kutta method is used for the time integration, shown as

$$Q^{(0)}=Q^n,\quad Q^{(1)}=Q^{(0)}-\alpha_1 \Delta t_i R Q^{(0)},\quad \cdots,\quad Q^{(k)}=Q^{(0)}-\alpha_k \Delta t_i R Q^{(k-1)},\quad Q^{n+1}=Q^{(k)} \qquad (4)$$

where α_k represents the kth stage coefficient and R is the residual. The standard stage coefficients and the approximate maximum CFL number are used.

Also the local time stepping and implicit residual smoothing was used to increase the convergence to the steady-state. The original residual R is smoothed by solving the implicit equations $\overline{R_i}=R_i+\varepsilon\nabla^2\overline{R_i}$, where $\nabla^2\overline{R_i}$ represents the undivided Laplacian of the residuals, and ε is a smoothing coefficient. A unity is used for ε, and a point Gauss-Seidel method is used with 2 or 3 iterations to obtain $\overline{R_i}$. In the study, the maximum CFL numbers are approximately doubled by using the implicit resdiual smoothing, and the CFL number of 5.5 is used for 4 stage Runge-Kutta method.

3. Numerical Results and Discussion

First, a lid-driven cavity flow in a rectangle is considered for Re=400, 1000, and 5000. Triangular meshes are generated by halving the quadrilaterals of a non-uniform structured grid, in order to have a consistency in comparing with the structured grid solutions. Here the equivalent mesh sizes of 30x30, 40x40, and 50x50 are used for the Reynolds numbers of 400, 1000, and 5000, respectively. Fig. 2 shows a non-uniform grid of 5000 elements (equivalent to 50x50 structured grid) and the stream function contours for Re=5000. Also the centerline u-velocity profiles of the present computation are compared with benchmark solutions (Ghia et al.[4], 256x256 grid) in Fig. 3. Agreement is generally quite good. A more detailed comparison is summarized in Table 1. The minimum u-velocity values and locations, and also the stream function values and locations of the primary and secondary vortices are compared. Agreement is excellent for Re=400 and 1000, although a little

discrepancy is observed for Re=5000.

The second case is a lid-driven cavity flow in a rectangle with three cylinders inside located diagonally. This is the case of a multi-body geometry, for which the unstructured mesh generation has advantages over the structured one. Fig. 4(a) shows the triangular meshes of 3616 elements and 1891 nodes generated by advancing front method[5]. For Re=100, 400, 800, and 2000, convergences are shown in Fig. 4(b) and (c). It seems that, with relatively a little bit irregularly distributed triangular meshes, practically dependable convergences are achieved. Streamline patterns of the flows are also well represented in Fig. 5(a)-(d) for each Reynolds number. Due to the results of the interaction with cylinders, the positions and deformed structures of the lid-generated primary vortex are quite differentiable among various Reynolds numbers.

The last case considered is a rotating lid-driven cylindrical cavity flow, where the Reynolds number based on a cylinder radius and an angular velocity is 1854, and a cylinder aspect ratio H/R is 2. An axisymmetric vortex breakdown at the rotation axis was observed in the experiment of Escudier[6]. Fig. 6 shows a convergence of the case, in which a transient vortex breakdown lasts a quite long period of time and a steady state was established at the iteration of 20000. The stream function contours in Fig. 7(a) are computed on triangular meshes with an equivalent size of 80x50. It has a good resemblance to the experiment shown in Fig. 7(b), comparing the location, shape and size of the bubble; h/H & s/H = 0.19 & 0.16 (present), 0.21 & 0.16 (exp.), and 0.20 & 0.14 (Ref. [7]), (h: bubble location from bottom, s: bubble size, and H: cylinder height).

Based on validations for three different types of incompressible laminar recirculating cavity flows, present numerical formulation seems to have a fairly competent accuracy and convergence property, compared with other incompressible Navier-Stokes solvers.

REFERENCES

[1] Chorin, A.J., "A Numerical Method for Solving Incompressible Viscous Flow Problems," J. Comp. Phys., Vol. 2, 1967.

[2] Kwak, D.C., Chang, L., Shanks, S., and Chakravarthy, S., "A Three-Dimensional Incompressible Navier-Stokes Equations," AIAA J., Vol. 24, No. 3, 1986.

[3] Holmes, D.G. and Connell, S.D., "Solution of the 2D Navier-Stokes Equations on Unstructured Adaptive Grids," AIAA 80-1932-CP, 1989.

[4] Ghia, U., Ghia, K.N., and Shin, C.T., "High-Re Solutions for Incompressible Flow Using the Navier-Stokes Equations and a Multigrid Method," J. Comp. Phys., Vol. 48, 1982.

[5] Peraire, J., Vahdati, M., Morgan, K., and Zienkiewicz, O., "Adaptive Remeshing for Compressible Flow Computations," J. Comp. Phys., Vol. 77, 1987.

[6] Escudier, M.P., "Observations of the Flow Produced in a Cylindrical Container by a Rotating Endwall," Exp. Fluids, Vol. 2, 1984.

[7] Lugt, H.J. and Abboud, M., "Axisymmetric Vortex Breakdown With and Without Temperature Effects in a Container with a Rotating Lid," J. Fluid Mech. Vol. 179, 1987.

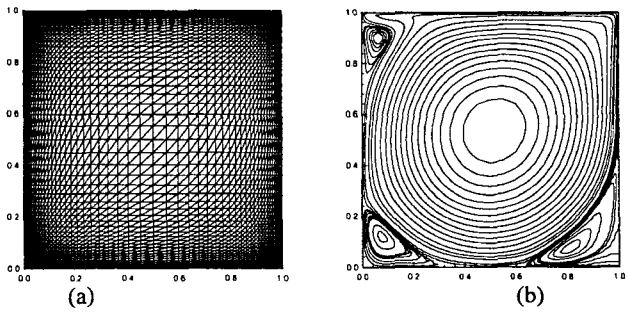

Fig 2. (a) equivalent mesh 50x50, (b) stream function contours, Re=5000.

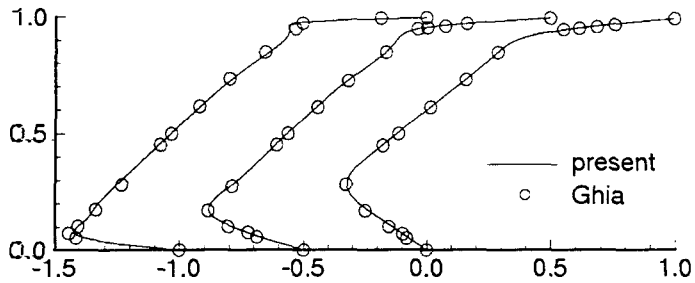

Fig 3. Centerline u-velocity comparison with benchmark solution: (a) equivalent mesh 30x30, Re=400, (b) 40x40, Re=1000, (c) 50x50, Re=5000 (from R to L).

		on vertical centerline		primary vortex			secondary vortex (bottom right)		
		U_{min}	y_{min}	Ψ	x	y	Ψ	x	y
Re=400	presen	-	0.2767	-	0.553	0.608	0.633×10^{-3}	0.892	0.1342
	Ghia	-	0.2770	-			0.642×10^{-3}		
Re=1000	presen	-	0.1737	-	0.532	0.566	0.144×10^{-2}	0.866	0.1100
	Ghia	-	0.1719	-	0.531	0.562	0.175×10^{-2}	0.859	0.1094
Re=5000	presen	-	0.0796	-	0.516	0.536	0.313×10^{-2}	0.805	0.0711
	Ghia	-	0.0703	-	0.511	0.535	0.308×10^{-2}	0.808	0.0742

Table 1. Comparison of solutions for Re=400, 1000, and 5000.

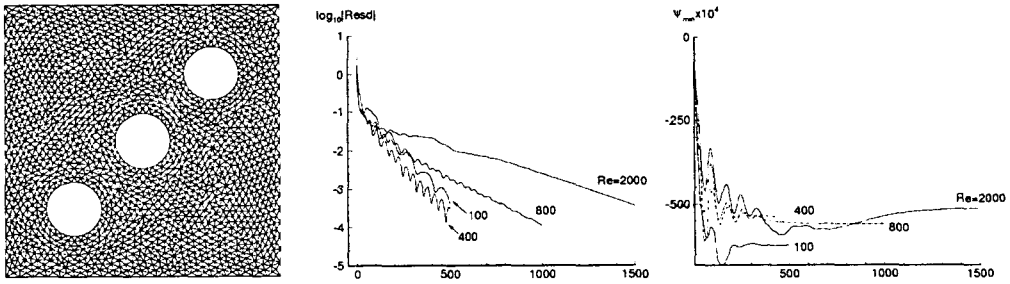

(a) (b) (c)

Fig. 4 Cavity flow with multiple cylinders: (a) mesh: 3616 elements, 1891 nodes, convergences: (b) u-momentum, (c) min stream function.

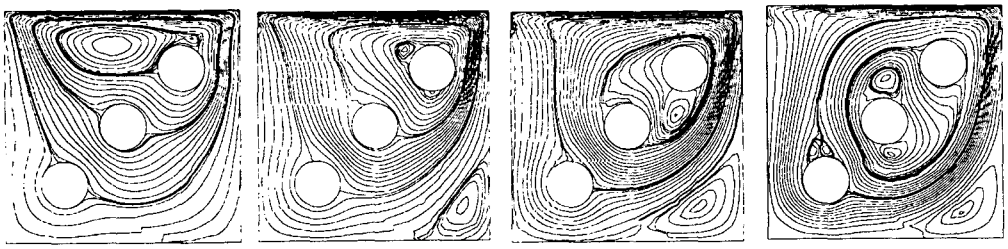

(a) Re=100 (b) Re=400 (c) Re=800 (d) Re=2000

Fig 5. Streamline patterns for various Reynolds numbers.

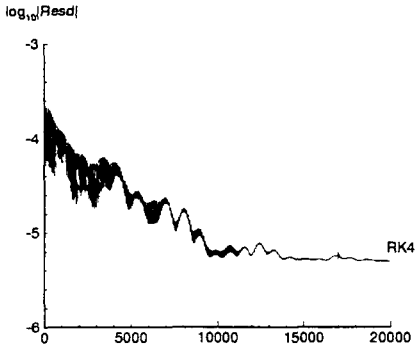

Fig. 6 Convergence of a cylindrically driven cavity flow

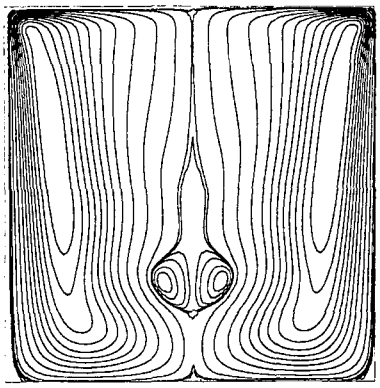

(a) stream function contours
(equivalent mesh 80x50)

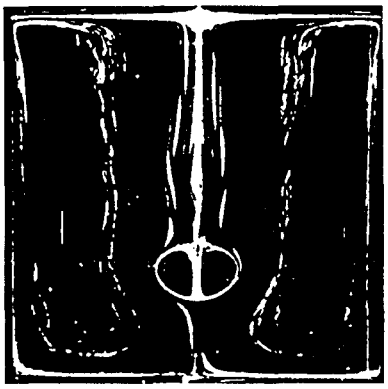

(b)

Fig. 7 (a) present computation, (b) experiment (by M. P. Escudier),
$Re = 1854$, $H/R = 2$.